Soft Matter

PAPER

View Article Online
View Journal | View Issue

Cite this: *Soft Matter*, 2026, **22**, 814

Collective filament wrapping and nested spiral formation in active polydisperse systems

Caterina Landi, [a] Giulia Janzen, [b] Francesco Sciortino, [c] John Russo, [c] Chantal Valeriani *[a] and Daniel A. Matoz-Fernandez *[b]

Received 31st July 2025,
Accepted 27th December 2025

DOI: 10.1039/d5sm00783f

rsc.li/soft-matter-journal

We investigate a two-dimensional polydisperse suspension of self-propelled semiflexible filaments and reveal a collective wrapping mechanism that is absent in monodisperse systems. At intermediate activity levels, long filaments coil around shorter ones, forming nested spiral structures stabilized by filament length disparity. These assemblies generalize the single-filament spiraling seen in active systems into cooperative, multi-filament configurations. As activity increases, the nested spirals undergo structural transitions: medium-length filaments unwind, longer filaments encapsulate shorter ones, and eventually all spiral structures dissolve. This reorganization is reflected in the dynamics, where van Hove distributions uncover coexisting confined and motile filament populations. Our findings identify filament length as a key control parameter for nonequilibrium self-assembly and establish inter-filament wrapping as a minimal mechanism for hierarchical organization in active matter. This mechanism provides a simple model for the cooperative confinement and structural hierarchy observed in both biological and synthetic active systems.

1 Introduction

Filamentous active systems are found across biology and synthetic materials, exhibiting rich dynamics driven by their elongated shape and self-propulsion.[1] In biological contexts, they include cytoskeletal filaments such as microtubules and actin,[2,3] as well as larger organisms like elongated bacteria[4–6] and worms.[7–9] Synthetic analogues range from active chains of metal-dielectric Janus particles under electric fields,[10] to vibrated granular rods with polymer-like behavior,[11,12] and robotic swarms designed for collective motion.[13,14]

Among the many collective behaviors exhibited by active filaments, the emergence of swirls, vortices, and spiral patterns stands out as particularly intriguing. In cytoskeletal systems, such patterns have been observed across a range of experimental setups,[15–18] often serving functional roles. For instance, cortical microtubules in plant cells organize into swirling arrays that guide anisotropic cell wall growth.[19] Similar spiral structures have also been reported in dense bacterial suspensions, where longer filamentous bacteria are surrounded by shorter ones,[20] highlighting the role of filament flexibility in spiral pattern formation.

Two-dimensional numerical simulations have shown that single self-propelled flexible filaments can spontaneously form stable spiral conformations.[21] When such filaments interact in monodisperse systems, increasing activity has been shown to trigger a transition from open-chain swimming to frozen spiral states,[22] which subsequently break apart at even higher activity levels.[23] The interplay between steric interactions and filament flexibility plays a crucial role in the formation of spirals: while stronger steric repulsion generally promotes alignment and long-range order, increased flexibility enables bending and self-contact, driving the spontaneous formation of persistent single-filament spirals.[24] Dense active filament systems highlight how steric crowding and flexibility together control the transition between collective flow and spiral-dominated phases.[25] Similar spiral conformations arise in a variety of active systems, including filaments propelled by explicit motor proteins,[26] partially active polymers,[27] polymers driven by tangential or push–pull activity,[28] and chains of chiral active Brownian particles,[29] indicating that spiral formation is a robust self-organization mechanism beyond the specific details of the propulsion. In three dimensions, rather than forming planar spirals, active filaments undergo coil-to-globule-like transitions[30] and reentrant swelling behavior.[31]

Despite the extensive phenomenology uncovered in active filament systems,[32] most theoretical and simulation studies to date have relied on monodisperse models, where all filaments share the same length. In contrast, real-world systems are inherently polydisperse. In biological contexts, filament length

[a] *Department of Structure of Matter, Thermal Physics, and Electronics, Complutense University of Madrid, Madrid 28040, Spain. E-mail: cvaleriani@ucm.es*
[b] *Department of Theoretical Physics, Complutense University of Madrid, Madrid 28040, Spain. E-mail: dmatoz@ucm.es*
[c] *Department of Physics, Sapienza Universitá di Roma, 00185 Rome, Italy*

varies due to dynamic processes such as polymerization, depolymerization, severing, and annealing,[33–35] while in engineered systems, both synthetic polymers[36] and self-morphic active materials[37] frequently display length heterogeneity.

Polydispersity introduces new forms of structural and dynamical heterogeneity, which can fundamentally alter collective behavior.[38,39] Yet its role in active filament systems remains largely unexplored. By explicitly incorporating length variability into our models, we aim to capture more realistic dynamics and reveal new mechanisms of self-organization. A recent study[40] demonstrated that active Brownian particles assembling into polydisperse chains exhibit distinct phase behavior—ranging from crystalline clusters to motility-induced spirals—depending on activity and temperature. However, because these chains form and break dynamically, their structural characterization remains challenging.

Motivated by the gap in understanding spiral formation under polydispersity, we study a system of tangentially self-propelled filaments with fixed bond lengths and tunable length distributions, as detailed in Section 2. Our goal is to investigate how filament length heterogeneity influences collective dynamics—particularly the formation, stability, and evolution of spiral structures. As shown in Section 3.1, polydispersity does not suppress spiral formation or the characteristic reentrant behavior observed in monodisperse systems. Instead, it shifts the transition thresholds for different filament lengths, enabling spiral configurations to persist at higher activity levels. This extended stability arises from a cooperative trapping mechanism, where long filaments dynamically wrap around and confine shorter ones. In Section 3.2, we demonstrate that increasing activity drives a gradual transition from multi-filament to two-filament nested spirals, reflecting the fact that filaments of different lengths unwind at different Péclet numbers. This structural reorganization is mirrored in the dynamics: van Hove displacement distributions reveal coexisting populations of confined and motile filaments, depending on their length and degree of entanglement.

Together, these findings show that polydispersity promotes a hierarchical mode of self-assembly, where structural diversity enables cooperative confinement and the stabilization of collective wrapping across activity regimes.

2 Model

We investigate a two-dimensional polydisperse system of self-propelled filaments to study how length heterogeneity affects their structural organization and dynamical behavior. Each filament is modeled as a linear chain of N_b active beads. The number of beads per filament remains fixed; filaments neither break nor recombine. The system is simulated in the dry limit, where long-range hydrodynamic interactions are neglected. The surrounding medium exerts only local friction and thermal noise. The motion of each bead follows the underdamped Langevin equation:[21,25]

$$m\ddot{\mathbf{r}}_i = -\gamma\dot{\mathbf{r}}_i + \mathbf{R}_i(t) + \sum_{j\neq i}\mathbf{f}_{ij} + \mathbf{f}_i^{a}, \quad (1)$$

where m and $\mathbf{r}_i$ represent the mass and the position in space of the bead i, dots indicate time derivatives, and γ is the damping coefficient. The term $\mathbf{R}_i(t)$ represents a delta-correlated random force, characterized by a zero mean and a variance of $4\gamma k_B T\delta_{ij}\delta(t-t')$, where k_B is the Boltzmann constant, and T is the temperature.

The interaction force is derived from the total potential $\phi(r_{ij})$, such that $\mathbf{f}_{ij} = -\nabla_i\phi(r_{ij})$, where $r_{ij} = |\mathbf{r}_i - \mathbf{r}_j|$. The total potential is decomposed as $\phi(r_{ij}) = \phi_B(r_{ij}) + \phi_{NB}(r_{ij})$, with ϕ_B accounting for bonded interactions and ϕ_{NB} for short-range non-bonded steric repulsion. Bonded interactions ϕ_B include a stretching contribution modeled *via* the Tether potential[41] and a bending contribution given by a harmonic angle potential,[25] such that $\phi_B = \phi_{bond} + \phi_{bend}$. Non-bonded interactions ϕ_{NB} are modeled *via* the Weeks–Chandler–Andersen (WCA) potential,[42] ensuring purely repulsive excluded-volume effects. All details related to the interaction parameters are provided in the SI.[43]

The self-propulsion force acting on bead i is defined as $\mathbf{f}_i^{a} = f_a\mathbf{t}_{i-1,i+1}$, where f_a is the propulsion strength, and $\mathbf{t}_{i-1,i+1} = \frac{\mathbf{r}_{i+1}-\mathbf{r}_{i-1}}{|\mathbf{r}_{i+1}-\mathbf{r}_{i-1}|}$ is a unit vector approximating the local backbone tangent.[30,44,45] End beads ($i = 1$ and $i = N_b$) do not experience propulsion, *i.e.*, $f_a = 0$ at the filament ends. Note that choosing the push–pull active polymer model[21,25] would yield similar results, provided the mean active force is appropriately normalized.[28]

Finally, the system contains $N = 5\times10^4$ particles of diameter σ. We consider filaments of various lengths, with the number of beads per filament given by $N_b \in \{3, 11, 20, 28, 37, 45, 54, 62, 71, 80\}$. The system contains an equal number of filaments for each length. A single filament may slightly deviate from this set to ensure that the total number of particles exactly matches N. We uniformly sample the filament lengths within the interval $3 \leq N_b \leq 80$ in order to explore the role of polydispersity without any length bias. The choice of this interval is inspired by the work of ref. 40, where active bifunctional Brownian particles self-assemble into chains reaching lengths comparable to those considered in our simulations.

The length of a filament is approximated as $L \approx b(N_b - 1)$, being $b = 0.86$ the bond reference length. The stiffness of each filament is characterized by the dimensionless persistence ratio $\xi_p/L = 2b\kappa/(Lk_BT)$, where κ is the bending rigidity. Solving for κ, we obtain $\kappa = (\xi_p/L)(LK_BT/2b)$. We set $\xi_p/L = 1.3$ for all filaments and determine the corresponding κ values accordingly. κ values are provided in the SI.[43]

The strength of active forcing relative to thermal noise is quantified by the Péclet number $\mathrm{Pe} = \frac{3f_a\sigma}{k_BT}$. To explore different activity regimes, we vary Pe at fixed packing fraction $\rho = 0.3$. Periodic boundary conditions are applied in both directions of the square box.

In this manuscript, all quantities are expressed in reduced units with $\sigma = 1.0$, $\varepsilon = 1.0$, and $m = 1.0$ (see SI[43] for a more precise definition of bead diameter σ and energy scale ε). Hence, time is expressed in units of $\tau = \sigma\sqrt{m/\varepsilon}$. The thermal energy is set to $k_BT = 0.1$, and the damping coefficient to $\gamma = 1.0$.

All simulations are carried out using the GPU-accelerated SAMoS molecular dynamics package,[46] with time integration performed using the BAOAB scheme for Langevin dynamics.[47] We set the integration time step to $\delta t = 10^{-3}$. For Pe $\geq$ 16.0, a smaller time step of $\delta t = 5 \times 10^{-4}$ is used to maintain numerical stability. We first let the system relax for 8×10^4 time steps, after which static properties are measured by averaging over 100 independent configurations sampled every 500 steps.

For further details, refer to the SI.[43]

3 Results and discussion

3.1 Structural characterization: turning number per filament length

To characterize the system's structural behavior, we compute the turning number[26,48] for each filament and then average these values over filaments of the same length. The turning number is defined as

$$\psi = \frac{1}{2\pi} \sum_{j=1}^{N_b-1} (\theta_{j+1} - \theta_j), \tag{2}$$

where $\theta_{j+1} - \theta_j$ represents the angular variation between two consecutive beads. This quantity measures the number of turns that a filament makes between its two ends: for an elongated filament, $|\psi| = 0$ (no turn); for a circular filament, $|\psi| = 1$ (one turn); and higher values of $|\psi|$ correspond to filaments in spiral configurations (more than one turn).

Fig. 1(a) shows the average turning number, $\langle|\psi|\rangle$, as a function of the Péclet number for five representative filament lengths: one short ($N_b = 11$), three medium ($N_b = 28$, $N_b = 37$ and $N_b = 54$), and one long ($N_b = 71$). Turning numbers for all other lengths are provided in the SI.[43] Here, $\langle\cdot\rangle$ denotes the ensemble average over all filaments of the same length. Short filaments ($N_b = 11$) exhibit a turning number close to zero across all Pe, reflecting their inability to form spiral structures. In contrast, medium and long filaments ($N_b \geq 28$) display a non-monotonic trend: the turning number increases at intermediate Pe, indicating the formation of spiral structures, and decreases at high Pe, indicating a transition back to elongated configurations. This reentrant behavior is consistent with the monodisperse case.[23] Fig. 1(a) further indicates that longer filaments require higher activity to undergo this transition, showing that filaments of different lengths transition at different Péclet numbers. Thus, polydispersity does not qualitatively alter the reentrant behavior observed in the monodisperse case, provided the filaments are sufficiently long to form spirals.

However, polydispersity shifts the activity level at which the transition occurs for each filament length compared to the monodisperse case. This is observed by comparing the results of the polydisperse system with those of the corresponding monodisperse systems at the same filament lengths (Fig. 1(b)).

In the monodisperse systems with relatively long filaments ($N_b = 54$ and $N_b = 71$ in Fig. 1(b)), no clear reentrant behavior is yet detected within the simulated range of Pe, whereas in the polydisperse system the transition has already begun.

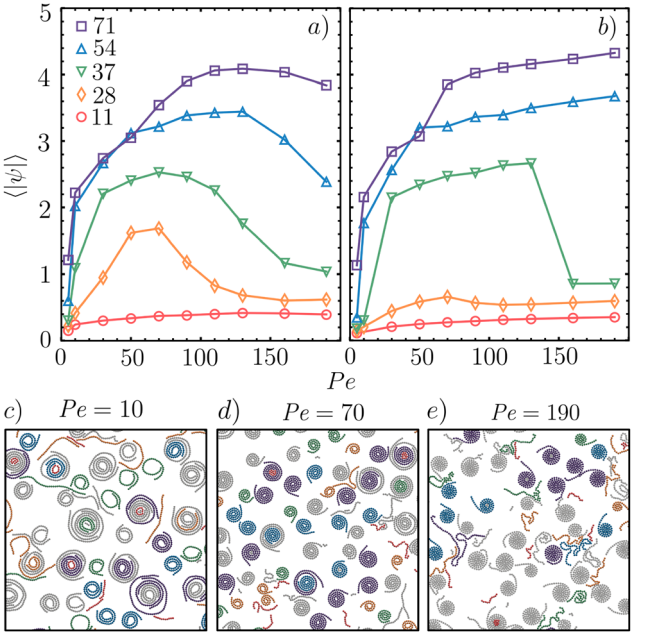

Fig. 1 Average turning number, $\langle|\psi|\rangle$, as a function of the Péclet number for different filament lengths: red circles for $N_b = 11$, orange diamonds for $N_b = 28$, green down triangles for $N_b = 37$, blue up triangles for $N_b = 54$, and purple squares for $N_b = 71$. While panel (a) illustrates the results for the polydisperse system, panel (b) shows for the corresponding monodisperse systems. (a) For short filaments ($N_b = 11$), the turning number remains close to zero across all Pe values, as the filaments are too short to form spiral structures. For longer filaments ($N_b \geq 28$), the turning number first increases and then decreases with Pe, indicating a reentrant behavior. The longer the filament, the higher the activity required to transition from an open-chain configuration to a tightly wound spiral configuration and back to an elongated one. (b) Qualitatively, the same reentrant behavior observed in the polydisperse system is recovered. Quantitatively, however, longer filaments ($N_b \geq 37$) require more time to unwind than in the polydisperse system, whereas most of the shorter filaments ($N_b = 28$) do not form spirals in regimes where they did so under polydisperse conditions. (c)–(e) Snapshots of the polydisperse system at steady-state: (c) at low (Pe = 10), (d) intermediate (Pe = 70), (e) and high Péclet number (Pe = 190). Filaments are colored according to the legend in the top panel. Filaments in gray correspond to those whose length is not reported in the top panel.

Specifically, at high activities (Pe $\gtrsim$ 150), where these long filaments still form stable spirals in the monodisperse system, the presence of short filaments already in an open-chain state perturbs their spiral configurations, promoting premature unwinding (see SI[43] for representative comparative snapshots). A similar anticipation of the transition is also observed for medium-long filaments ($N_b = 37$), which do undergo the transition within the studied Pe range.

For medium-short filaments ($N_b = 28$), polydispersity promotes spiral formation, as indicated by a higher average turning number than in the monodisperse case where spirals, if they form, must be few relative to the total number of filaments (see SI[43] for the fraction of spirals in the monodisperse and polydisperse systems). In the polydisperse system, at lower activities (Pe $\approx$ 10–30), short filaments can be assisted in the spiral formation by nearby longer filaments which are already

in loose spiral configurations and can coil around them (see SI[43] for the fraction of spirals that are part of nested spirals in the polydisperse system). At higher activities (Pe ≈ 50–90), the presence of spirals among short filaments can also be facilitated by the fact that longer chains are in stable, compact and slow spiral configurations, which reduces disturbances and allows smaller filaments to maintain their spiral structures (see SI[43] for representative comparative snapshots).

All these observations highlight a dual effect of polydispersity depending on filament length. For longer filaments, polydispersity anticipates the reentrant spiral-to-open transition, while for short filaments it instead promotes the stabilization of spirals that would otherwise not emerge with this intensity in the monodisperse system due to their intrinsic size-related instability. Length heterogeneity facilitates the onset of the reentrant transition for medium and long filaments, likely by enabling interactions between filaments of different stability and coiling state. In the monodisperse case, filaments of equal length undergo the spiral-to-open transition simultaneously at a well-defined activity level. In contrast, in the polydisperse system, this transition is staggered: shorter chains unwind earlier, while longer chains remain spirals until higher Péclet numbers. The coexistence of open short chains and still-spiral long chains introduces additional interactions in the system. Consequently, the transition for long filaments becomes anticipated. Length heterogeneity facilitates spiral formation in short filaments thanks to the presence of longer filaments in spiral states. At lower activities, when these longer filaments are in loose spiral states, they wrap around shorter ones and assist their spiral formation. At higher activities, when the longer filaments adopt more compact spiral states, they provide a stable environment that allows shorter filaments to maintain their spiral structures.

We also tested an exponentially decaying filament length distribution, inspired by the self-assembly of active bifunctional Brownian particles,[40] and arguably more biologically relevant.[49–52] Such a distribution inherently yields very uneven statistics, with short filaments being abundant and long ones rare, which prevents a systematic quantitative comparison. The results are qualitatively similar to those obtained with a uniform distribution (see SI[43]); therefore, we hereby focus on the uniform case.

The structural phases described above are illustrated in the system snapshots shown in Fig. 1(c)–(e). At low Pe (Fig. 1(c)), filaments loosely wind into spiral structures. As Pe increases (Fig. 1(d)), these spirals become more tightly wound. Finally, at high Pe (Fig. 1(e)), only long filaments form tightly wound spirals, while shorter filaments are fully unwound. Notably, Fig. 1(c)–(e) also shows that, regardless of Pe, the system contains not only individual spiral filaments but also clusters of filaments that are interwound or wrapped around each other.

Such structures also appear in the monodisperse case;[22] however, while in monodisperse systems they vanish at high Pe, they persist longer in the polydisperse case. This persistence arises from longer filaments, not yet uncoiled, winding around shorter ones (Fig. 1(e)). Eventually, at very high Pe, even these two-filament structures break down, as long filaments also uncoil. In the next section (Section 3.2), we characterize these 'nested' structures using both structural and dynamical measurements.

3.2 Nested spirals as emergent collective structures

The coiling behavior of filaments at intermediate activities (Fig. 1) coexists with the formation of structurally organized assemblies, driven by filament–filament interactions. These assemblies consist of clusters of interlocking filaments arranged in spiral configurations, in agreement with the observations reported in ref. 22. Although filament roughness can, in principle, enhance interlocking between neighboring chains, we expect that smoother filaments would display a qualitatively similar behavior, with only minor differences in the stability and lifetime of spiral configurations.[21,22] We refer to these collective structures as nested spirals, defined as clusters in which the centers of mass of all constituent filaments lie within a threshold distance $\bar{r}$. The exact threshold value (with an analysis of its variation) and a detailed explanation of the identification procedure are provided in the SI.[43]

Fig. 2 shows an example of how a nested spiral forms. The process begins with open-chain configurations (Fig. 2(a)), and

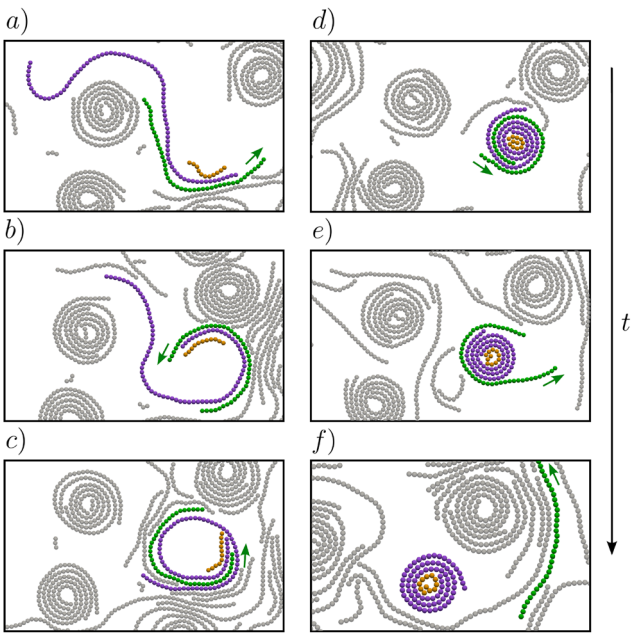

Fig. 2 Snapshots illustrating the typical mechanism of formation (a)–(d) and transition to a two-filament state of a nested spiral (e) and (f). Snapshots show a short (orange), a medium (green), and a long (purple) filament during system equilibration at Pe = 10. (a) Filaments start in open-chain configurations. (b) Driven by activity, the medium and long filaments begin to coil, initiating spiral formation. (c) As they coil, they capture and incorporate the smaller filament encountered along the way, forming a nested structure. (d) The nested structure becomes more compact, providing a relatively stable configuration for the long filament. (e) The medium filament becomes unstable and uncoils. (f) This results in a two-filament nested spiral composed of a long and a short filament. The green arrow in each panel indicates the self-propulsion direction of the medium filament.

as activity drives motion, medium and long filaments begin to coil, initiating spiral formation (Fig. 2(b)). During this stage, smaller filaments become trapped in the coiling structure, leading to the formation of a loose nested spiral (Fig. 2(c)). This nested structure then transitions to a more stable configuration, in which filaments are more tightly wound (Fig. 2(d)). However, depending on the activity, medium filaments may become unstable and uncoil (Fig. 2(e)), ultimately leading to a two-filament nested spiral composed of one long and one short filament (Fig. 2(f)). We anticipate that, at higher activities, even these two-filament structures eventually break down, as long filaments uncoil, and return to an open-chain state.

The structure and composition of nested spirals vary markedly with increasing activity. We begin by examining the average number of filaments per nested spiral, $\langle N_f \rangle$. As shown in Fig. 3(a), at low Pe, nested spirals typically comprise more than two filaments, while at high Pe, the average converges to two, indicating that they ultimately consist of filament pairs. This trend is further supported by the probability distributions of the number of filaments per nested spiral across different Pe (see SI[43]). Moreover, the filament lengths involved in these nested structures change with the Péclet number. This effect is quantified by measuring the average ratio of the shortest, $l_{\min}$, to the longest filament, $l_{\max}$, in each structure, $\langle l_{\min}/l_{\max} \rangle$ (Fig. 3(b)). At low Pe, this ratio is close to one, indicating that nested spirals are typically composed of filaments of similar length. As Pe increases, this ratio decreases toward its minimum, reflecting a transition to structures formed by one short and one long filament. What we observe here is consistent with the monodisperse case:[22] as Pe increases, nested spirals composed of filaments of similar lengths progressively disappear. Additionally, long filaments dominate at low Pe, as indicated by the increased average filament length in this regime (see SI[43]). Overall, as the Péclet number increases, nested spirals transition from a state in which they typically consist of multiple long filaments to one where they are composed of only two filaments, one long and one short.

These results highlight a second key effect of polydispersity: it stabilizes the presence of nested spiral at high Pe by facilitating a trapping mechanism between filaments of different lengths. Longer filaments can wrap around shorter ones, preventing their escape and maintaining the integrity of the nested structure. The coexistence of short and long filaments thus promotes the persistence of nested spirals well beyond the regime where they typically vanish in monodisperse systems. In addition, short filaments themselves benefit from this trapping mechanism, as the confinement imposed by longer chains helps them to remain in a coiled state.

Finally, we observe that the number of nested spirals, N_{nested}, initially increases with activity and then decreases, as shown in Fig. 3(c). This decrease exhibits a two-stage behavior: a rapid initial decay followed by a more gradual reduction, reflecting the formation and disruption mechanisms of nested spirals described earlier (Fig. 2). At low Pe, multi-filament nested spirals are common, as medium and long filaments tend to form coiled structures (Fig. 3(d)). As Pe increases,

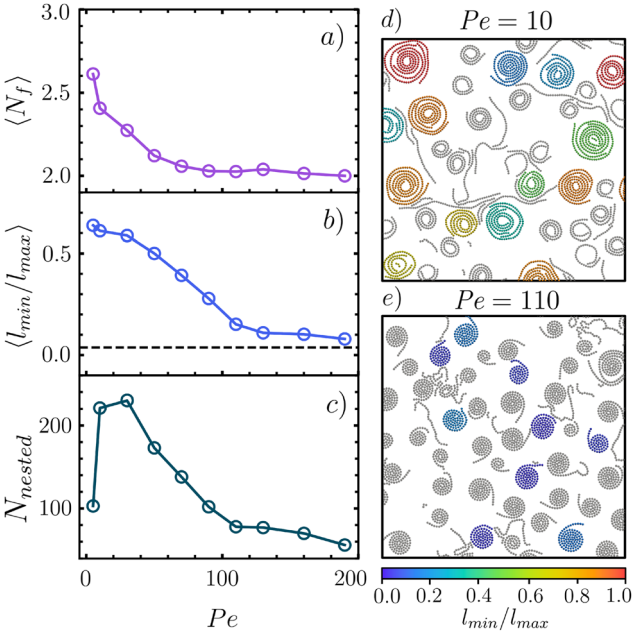

Fig. 3 Structural properties of nested spirals as a function of the Péclet number. Panels (a) and (b) report ensemble-averaged quantities computed over all identified nested spirals. (a) Average number of filaments per nested spiral, $\langle N_f \rangle$. At low Pe, nested spirals typically contain more than two filaments, while at high Pe, they are predominantly composed of filament pairs. (b) Average length ratio of the shortest to the longest filament in each nested spiral, $\langle l_{\min}/l_{\max} \rangle$. The dashed black line at $y = 3/80$ denotes the minimum possible ratio based on the set of filament lengths in the system. At low Pe, filaments within nested spirals tend to be of similar length, while at high Pe, they exhibit pronounced length disparity. (c) Total number of nested spirals, N_{nested}. This quantity increases at low activity, reaches a peak, and then decreases with further increasing Pe. The decrease occurs in two stages: a sharp decay for $30 < \text{Pe} \leq 110$, followed by a more gradual reduction for $\text{Pe} > 110$. Initially, nested spirals form from the winding of medium and long filaments ($\text{Pe} \leq 30$). As Pe increases, medium filaments begin to unwind, breaking apart multi-filament spirals. Concurrently, long filaments wrap around short filaments, forming predominantly two-filament nested spirals. At high Pe, these structures dissolve as long filaments themselves unwind. (d) and (e) Representative snapshots of the system in steady state at Pe = 10 (d) and Pe = 110 (e). Filaments belonging to nested spirals are colored according to the length ratio $l_{\min}/l_{\max}$ of the corresponding structure. Filaments not participating in nested spirals are shown in gray.

medium filaments progressively unwind, destabilizing these structures. This results in a transient regime where two-filament nested spirals dominate, typically formed by a long filament wrapping around a short one (Fig. 3(e)). At even higher Pe, long filaments also unwind, leading to the eventual breakdown of nested spirals.

In addition, the SI reports the probability distribution of the normalized lifetime of nested spirals (τ_s), showing that these structures remain stable within the simulated time window. This suggests that unwinding most likely occurs during the equilibration stage after increasing Pe.

To isolate the effect of polydispersity, the persistence ratio ξ_p/L was kept fixed throughout the previous analysis. In what follows, we are going to vary the persistence length and construct a phase

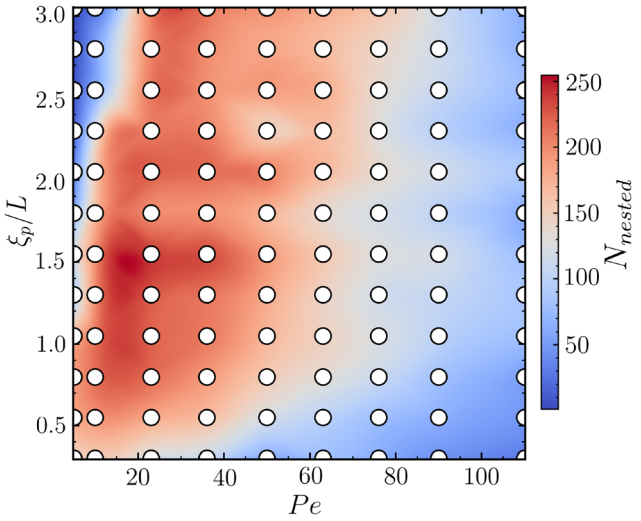

Fig. 4 Number of nested spirals in the (Pe, ξ_p/L) plane. The number of nested spirals presents a reentrant behavior with increasing Pe for almost all values of ξ_p/L. While qualitatively the reentrant behavior is unvaried when varying ξ_p/L, activities at which nested spirals appear and disappear are affected by it. Specifically, the lower ξ_p/L, the lower Pe at which nested spirals emerge, since more flexible filaments require less activity to coil. For the same reason, at lower ξ_p/L, nested spirals also break up at lower Pe, since filament flexibility promotes the transition to compact and single-filament spiral states.

diagram in the (Pe, ξ_p/L) plane to systematically assess its influence on the nested spirals formation (see Fig. 4).

The phase diagram shows that, for all ξ_p/L considered, the system exhibits the reentrant behavior described in Fig. 3(c): nested spirals are absent at high Pe (in blue) and only appear at intermediate Pe (in red), where filaments can coil efficiently without becoming unstable. Moreover, the lower the persistence ratio, the earlier nested spirals emerge, since more flexible filaments require less activity to coil (in agreement with ref. 25). At low persistence ratios, nested spirals also disassemble at lower Pe, as filaments are flexible enough to transition to compact and single-filament spiral states with less activity.

The structural reorganization of filaments into nested spirals has a strong impact on their dynamics. In particular, the formation of nested spirals gives rise to distinct displacement behaviors that depend on filament length and structural organization. To quantify these effects, we analyze the self-part of the van Hove distribution,[53,54] which describes the probability distribution of filament displacements. Specifically, it measures how far the center of mass of each filament has moved after a time lag Δt. The van Hove distribution is defined as

$$G_s(\Delta r;\Delta t) = \left\langle \frac{1}{N_f^{tot}} \sum_{i=1}^{N_f^{tot}} \delta\left(\Delta r - \left|\mathbf{r}_i^{cm}(t+\Delta t) - \mathbf{r}_i^{cm}(t)\right|\right) \right\rangle, \quad (3)$$

where N_f^{tot} is the total number of filaments in the system, $\mathbf{r}_i^{cm}(t)$ denotes the position of the center of mass of filament i at time t, Δr represents the magnitude of the displacement between time t and time $t+\Delta t$, and $\delta(\ldots)$ is the Dirac delta function. The time average $\langle\cdot\rangle$ is computed over a single simulation trajectory using $t = n\Delta t$, with n = 0, 1, 2, 3, 4, and 5, after equilibration. In addition, we average over 10 independent simulations with different random seeds. We compute this distribution for different filament lengths at Pe = 110 and show these values in Fig. 5 for two representative lag times: a short lag time, Δt = 1.5, and a longer one, Δt = 150. The Péclet number is set to Pe = 110, corresponding to an activity at which the transition to two-filament nested spirals has just occurred (Fig. 3).

Short filaments (Fig. 5(a) and (b)) exhibit a bimodal structure at both Δt = 1.5 and Δt = 150, indicating the coexistence of two distinct dynamic behaviors. This is reflected in the presence of two peaks in the displacement distribution: one at smaller Δr and one at larger Δr. The peak at larger Δr corresponds to filaments in elongated configurations undergoing directed motion, while the peak at smaller Δr arises from filaments incorporated into nested spiral structures. These

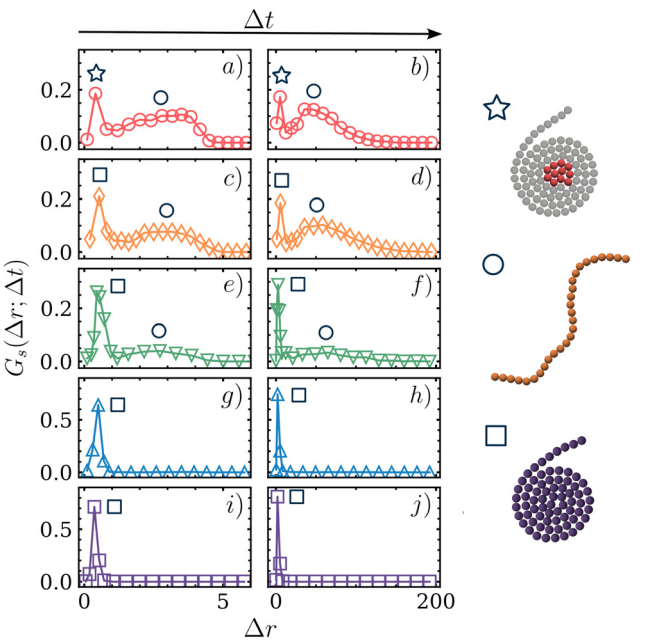

Fig. 5 van Hove distribution for filaments of different lengths at Pe = 110. Each pair of panels corresponds to a filament length: red circles for N_b = 11 (a) and (b), orange diamonds for N_b = 28 (c) and (d), green downward triangles for N_b = 37 (e) and (f), blue upward triangles for N_b = 54 (g) and (h), and purple squares for N_b = 71 (i) and (j). Left panels (a), (c), (e), (g) and (i) correspond to a short time, Δt = 1.5, while right panels (b), (d), (f), (h) and (j) correspond to a longer time, Δt = 150. (a) and (b) The distribution for short filaments (l = 11) displays a clear bimodal structure, indicating the presence of two distinct dynamical populations: one corresponding to filaments in elongated, motile configurations and another to filaments confined within nested spirals. When encapsulated by longer filaments, short filaments inherit the constrained dynamics of the nested structure. (c)–(f) Medium-length filaments (N_b = 28, N_b = 37) also exhibit a bimodal distribution, reflecting their coexistence in both spiral and elongated states. At this activity, medium filaments begin to unwind, resulting in a mixture of dynamical behaviors within the population. (g)–(j) For long filaments (N_b = 54, N_b = 71), the distribution shows a single peak, indicating a single dynamical mode. At this activity, long filaments are tightly wound and display a single, confined dynamical mode, either as isolated spirals or as part of nested structures.

confined filaments behave like spirals and exhibit limited mobility, resulting in smaller displacements. A similar bimodal distribution is observed for medium filaments (Fig. 5(c)–(f)), but the origin of this behavior is different. In this case, the filament length is sufficient to form spirals, but at this Péclet number some spirals, whether single or nested, begin to unwind. As a result, medium filaments can be found in either spiral or open-chain configurations, each associated with distinct displacement statistics. In contrast, the distribution for long filaments (Fig. 5(g)–(j)) displays a single peak, consistent with the fact that these filaments are mainly in tightly wound spiral conformations at this activity level, either as one filament spirals or part of nested spirals. In both cases, their dynamics is similarly constrained and do not exhibit the fast, directed motion characteristic of open-chains. Across all filament lengths, we observe consistent dynamical behavior at both short (Fig. 5(a), (c), (e), (g) and (i)) and long times (Fig. 5(b), (d), (f), (h) and (j)), indicating that the underlying dynamics is robust over time.

The van Hove function analysis goes beyond the expected observation that spiral structures move more slowly. In particular, it highlights that short filaments display a clear bimodal displacement distribution as a consequence of being trapped by longer, slowly moving spiral chains that wrap around them. These interactions generate two distinct dynamical populations within the short-filament ensemble: freely moving open chains and trapped filaments behaving as part of nested spirals. The van Hove analysis thus provides quantitative evidence for the formation of such wrapped configurations and their impact on the dynamics of the system elements.

The mean-square displacement of short filaments at different Péclet numbers is reported in the SI,[43] where it confirms the expected average scaling behavior but fails to capture the above described dynamical heterogeneity of short filaments.

4 Conclusions

In summary, our work shows that while a system composed of a distribution of polymer lengths behaves qualitatively similarly to a monodisperse system, some differences still emerge.

Understanding how structural diversity influences collective behavior in active matter is key to bridging idealized models and real-world systems, where heterogeneity is often unavoidable. In this work, we investigated how filament length polydispersity affects the self-organization of active semiflexible filaments. Our work demonstrates that while nested spiral structures can form in both monodisperse and polydisperse systems, polydispersity profoundly alters their stability and organization, promoting hierarchical wrapping and persistent confinement at high activity. These effects arise from dynamic interactions across length scales: long filaments can trap and stabilize shorter ones, extending the lifetime and robustness of spiral assemblies beyond what is observed in monodisperse populations.

In particular, by varying the Péclet number, we observe the same structural phases seen in the monodisperse case:[22,23,25] a polymer melt phase at low Pe, a transition to a pure spiral phase at intermediate Pe, and a reentrant unwinding of spirals at high Pe. Thus, polydispersity does not fundamentally alter the reentrant behavior observed in the monodisperse case,[23] provided filaments are sufficiently long to form spirals. However, it can shift the Pe at which these transitions occur. For relatively long filaments (N_b = 54 and N_b = 71), the transition appears anticipated in the polydisperse system, as in the monodisperse case it is not yet observed at the highest simulated values of Pe. A similar anticipation is found for medium-long filaments (N_b = 37), which exhibit the transition within the simulated Pe range. This occurs because, at Pe values where spirals are stable in the monodisperse system, the coexistence with shorter motile chains (already open) introduces additional interactions that destabilize the spiral configurations of longer filaments, leading to their premature unwinding. This behavior arises because filaments of different lengths respond differently to activity, causing the onset of the reentrant phase to extend over a range of Pe rather than occurring at a single threshold, making the transition staggered across filament lengths. This effect promotes the early onset of the reentrant behavior in mixed-length populations. At the same time, medium-short filaments (N_b = 28), which would remained open in the monodisperse system, can instead form and maintain spiral states in the polydisperse case, thanks to the presence of longer and still-coiled neighboring filaments.

Moreover, in monodisperse systems, it has been shown that at intermediate Pe, filaments can form interlocked or wrapped configurations, *i.e.*, nested spirals. However, these structures disappear as Pe increases.[22] In the polydisperse case, by contrast, such nested structures persist even at high Péclet numbers. As in the monodisperse case, nested spirals composed of filaments of comparable length vanish at high Pe. In the very high Pe regime, the most common nested spirals consist of a long filament wrapped around a much shorter one. This occurs because short filaments become trapped inside the tightly coiled spirals. We anticipate that at even higher Pe, these nested structures will eventually break down as the long filaments themselves uncoil and transition to open-chain configurations.

Nested spirals emerge in a comparable activity regime with ref. 23, once the different definitions of the Péclet number and the activity models (push–pull *versus* tangential) are taken into account.[28] Unlike the monodisperse case, where single spirals dominate at high Pe, polydispersity broadens the stability range of nested spiral structures by enabling the formation of two-filament nested spirals, with longer filaments enclosing shorter ones.

This dual role of polydispersity highlights its non-trivial impact on active filament self-organization. On one hand, heterogeneity enhances structural resilience by stabilizing the presence of nested spiral assemblies at high activity; on the other hand, it destabilizes long filament spirals at high activity, where the motion of short filaments in an open-chain state promotes their premature unwinding, and at the same time enable short filaments, which would remain open in monodisperse systems, to form and maintain spiral configurations

due to their interactions with the more stable longer coiled chains. Both effects emphasize that polydispersity is not a mere perturbation to an idealized model, but a key factor shaping the stability of emergent states in active filamentous matter.

Finally, we analyzed the dynamics of nested spirals with the van Hove distribution. For short filaments the distribution is bimodal, revealing two distinct dynamical behaviors: filaments trapped inside nested spirals show small displacements characteristic of confined spirals, whereas open-chain filaments move more freely and display larger displacement. Medium filaments exhibit a similar bimodal profile because, at this Péclet number, they begin to unwind and can exist either in spiral (single or nested) or open-chain configurations. In contrast, long filaments remain almost exclusively in tightly wound spiral conformations, leading to a single narrow peak in the van Hove distribution that reflects their constrained dynamics.

We discuss possible experimental implications and extensions of this work. A potential extension of this work would be to introduce length-dependent propulsion, allowing filaments of different lengths to self-propel at different speeds.[40] This modification would better reflect biological conditions and further clarify the role of polydispersity in active filament systems.

From an experimental perspective, synthetic colloidal polymers provide a promising platform for testing our predictions.

Synthetic colloidal (passive) polymers have been built in the laboratory to form either chains or rings,[55] with the goal of designing materials with multifunctional switchable properties.[56] To this day, experiments on active polymer chains or rings have been reported only by few authors. Wei and Kraft[57] have built micrometer-scale polymer integrating activity and flexibility. The structures are actuated by an AC electric field and display rotation, beating mechanism and undulatory locomotion, besides an emergent sense-response ability.

In this context, our numerical results may serve as guidance for experiments on synthetic active polymers whose shapes adapt to their environment. Introducing length polydispersity emerge as an effective strategy to promote inter-filament wrapping and nested spiral formation. The resulting cooperative multi-filament structures could potentially be exploited in applications such as active mixing or transport at the microscale.

Conflicts of interest

There are no conflicts to declare.

Data availability

Additional information about the model, and additional measurements to characterize the nested spirals are provided. Supplementary information is available. See DOI: https://doi.org/10.1039/d5sm00783f.

The data supporting the findings of this study are available from the corresponding author upon reasonable request.

Acknowledgements

DMF and GJ acknowledge support from the Comunidad de Madrid and the Complutense University of Madrid (Spain) through the Atracción de Talento program (Grant No. 2022-T1/TIC-24007). DMF also acknowledges support from MINECO (Grant No. PID2023-148991NA-I00). C. V. acknowledges fundings IHRC22/00002 and Proyecto PID2022-140407NB-C21 funded by MCIN/AEI/10.13039/501100011033 and FEDER, UE.

References

1 M. te Vrugt and R. Wittkowski, *Eur. Phys. J. E:Soft Matter Biol. Phys.*, 2025, **48**, 12.
2 A. Sciortino, H. A. Faizi and D. A. Fedosov, *et al.*, *Nat. Phys.*, 2025, **21**, 799–807.
3 S. Ganguly, L. S. Williams, I. M. Palacios and R. E. Goldstein, *Proc. Natl. Acad. Sci. U. S. A.*, 2012, **109**, 15109–15114.
4 Y. I. Yaman, E. Demir, R. Vetter and A. Kocabas, *Nat. Commun.*, 2019, **10**, 1–9.
5 S. S. Ding, L. J. Schumacher, A. E. Javer, R. G. Endres and A. E. Brown, *eLife*, 2019, **8**, e43318.
6 G. K. Auer, P. M. Oliver, M. Rajendram, T.-Y. Lin, Q. Yao, G. J. Jensen and D. B. Weibel, *mBio*, 2019, **10**, e00210–e00219.
7 A. Deblais, A. Maggs, D. Bonn and S. Woutersen, *Phys. Rev. Lett.*, 2020, **124**, 208006.
8 A. Deblais, S. Woutersen and D. Bonn, *Phys. Rev. Lett.*, 2020, **124**, 188002.
9 C. Nguyen, Y. Ozkan-Aydin, H. Tuazon, D. I. Goldman, M. S. Bhamla and O. Peleg, *Front. Phys.*, 2021, **9**, 734499.
10 J. Yan, M. Han, J. Zhang, C. Xu, E. Luijten and S. Granick, *Nat. Mater.*, 2016, **15**, 1095–1099.
11 P.-P. Wen, N. Zheng, L.-S. Li, H. Li, G. Sun and Q.-F. Shi, *Phys. Rev. E:Stat., Nonlinear, Soft Matter Phys.*, 2012, **85**, 031301.
12 B. W. Soh, I. R. Gengaro, A. R. Klotz and P. S. Doyle, *Phys. Rev. Res.*, 2019, **1**, 033194.
13 H. Marvi, C. Gong, N. Gravish, H. Astley, M. Travers, R. L. Hatton, J. R. Mendelson III, H. Choset, D. L. Hu and D. I. Goldman, *Science*, 2014, **346**, 224–229.
14 Y. Ozkan-Aydin, D. I. Goldman and M. S. Bhamla, *Proc. Natl. Acad. Sci. U. S. A.*, 2021, **118**, e2010542118.
15 L. Bourdieu, T. Duke, M. B. Elowitz, D. A. Winkelmann, S. Leibler and A. Libchaber, *Phys. Rev. Lett.*, 1995, **75**, 176–179.
16 V. Schaller, C. Weber, C. Semmrich, E. Frey and A. R. Bausch, *Nature*, 2010, **467**, 73–77.
17 Y. Sumino, K. H. Nagai, Y. Shitaka, D. Tanaka, K. Yoshikawa, H. Chaté and K. Oiwa, *Nature*, 2012, **483**, 448–452.
18 A. Sciortino and A. R. Bausch, *Proc. Natl. Acad. Sci. U. S. A.*, 2021, **118**, e2017047118.
19 J. Chan, G. Calder, S. Fox and C. Lloyd, *Nat. Cell Biol.*, 2007, **9**, 171–175.
20 S.-N. Lin, W.-C. Lo and C.-J. Lo, *Soft Matter*, 2014, **10**, 760–766.
21 R. E. Isele-Holder, J. Elgeti and G. Gompper, *Soft Matter*, 2015, **11**, 7181–7190.
22 O. Duman, R. E. Isele-Holder, J. Elgeti and G. Gompper, *Soft Matter*, 2018, **14**, 4483–4494.

23 G. Janzen and D. A. Matoz-Fernandez, *Soft Matter*, 2024, **20**, 6618–6626.
24 J. M. Moore, T. N. Thompson, M. A. Glaser and M. D. Betterton, *Soft Matter*, 2020, **16**, 9436–9442.
25 K. R. Prathyusha, S. Henkes and R. Sknepnek, *Phys. Rev. E*, 2018, **97**, 022606.
26 A. Shee, N. Gupta, A. Chaudhuri and D. Chaudhuri, *Soft Matter*, 2021, **17**, 2120–2131.
27 M. Vatin, S. Kundu and E. Locatelli, *Soft Matter*, 2024, **20**, 1892–1904.
28 G. Janzen, J. P. Miranda, J. Martín-Roca, P. Malgaretti, E. Locatelli, C. Valeriani and D. A. M. Fernandez, *J. Chem. Phys.*, 2025, **162**, 114905.
29 S. K. Anand, *J. Phys.: Condens. Matter*, 2025, **37**, 185101.
30 V. Bianco, E. Locatelli and P. Malgaretti, *Phys. Rev. Lett.*, 2018, **121**, 217802.
31 J.-X. Li, S. Wu, L.-L. Hao, Q.-L. Lei and Y.-Q. Ma, *Phys. Rev. Res.*, 2023, **5**, 043064.
32 R. G. Winkler and G. Gompper, *J. Chem. Phys.*, 2020, **153**, 040901.
33 A. Gopinathan, K.-C. Lee, J. M. Schwarz and A. J. Liu, *Phys. Rev. Lett.*, 2007, **99**, 058103.
34 D. Pavlov, A. Muhlrad, J. Cooper, M. Wear and E. Reisler, *J. Mol. Biol.*, 2007, **365**, 1350–1358.
35 D. Humphrey, C. Duggan, D. Saha, D. Smith and J. Käs, *Nature*, 2002, **416**, 413–416.
36 J. J. Lietor-Santos, C. Kim, M. L. Lynch, A. Fernandez-Nieves and D. A. Weitz, *Langmuir*, 2010, **26**, 3174–3178.
37 M. Kumar, A. Murali, A. G. Subramaniam, R. Singh and S. Thutupalli, *Nat. Commun.*, 2024, **15**, 4903.
38 J. Li, C. Zhang, Q. Zhang, S. Wang, R. Zhang, Z. Ding and Y. Han, *Macromolecules*, 2025, **58**, 3208–3220.
39 C. A. De Filippo, S. Del Galdo, P. Corsi, C. De Michele and B. Capone, *Soft Matter*, 2023, **19**, 1732–1738.
40 C. Landi, J. Russo, F. Sciortino and C. Valeriani, *Soft Matter*, 2025, **21**, 45–54.
41 H. Noguchi and G. Gompper, *Phys. Rev. E:Stat., Nonlinear, Soft Matter Phys.*, 2005, **72**, 011901.
42 J. D. Weeks, D. Chandler and H. C. Andersen, *J. Chem. Phys.*, 1971, **54**, 5237–5247.
43 Supplementary Material.
44 H. Jiang and Z. Hou, *Soft Matter*, 2014, **10**, 1012–1017.
45 M. Foglino, E. Locatelli, C. A. Brackley, D. Michieletto, C. N. Likos and D. Marenduzzo, *Soft Matter*, 2019, **15**, 5995–6005.
46 R. Sknepnek, *SAMoS: Self-propelled Agent-based Models with SAMoS*, https://github.com/sknepneklab/SAMoS, 2024, Accessed: 2024-04-29.
47 B. Leimkuhler and C. Matthews, *Molecular Dynamics: With Deterministic and Stochastic Numerical Methods*, Springer International Publishing, 2015.
48 S. G. Krantz, *Handbook of Complex Variables*, Birkhäuser, Boston, MA, 1st edn, 1999.
49 T. Mitchison and M. Kirschner, *Nature*, 1984, **312**, 237–242.
50 J. Howard and A. A. Hyman, *Nature*, 2003, **422**, 753–758.
51 A. Wegner, *J. Mol. Biol.*, 1976, **108**, 139–150.
52 T. D. Pollard and G. G. Borisy, *Cell*, 2003, **112**, 453–465.
53 J.-P. Hansen and I. R. McDonald, *Theory of Simple Liquids*, Academic Press, London, 2nd edn, 1986.
54 J. Helfferich, J. Brisch, H. Meyer, O. Benzerara, F. Ziebert, J. Farago and J. Baschnagel, *Eur. Phys. J. E:Soft Matter Biol. Phys.*, 2018, **41**, 71.
55 R. Verweij, J. Melio, I. Chakraborty and D. Kraft, *Phys. Rev. E*, 2023, **107**, 034602.
56 S. Liu, S. Murata and I. Kawamata, *Micromachines*, 2020, **11**, 987.
57 M. Wei and D. Kraft, *arXiv*, 2025, preprint, arXiv:2506.15198, DOI: 10.48550/arXiv.2506.15198.

